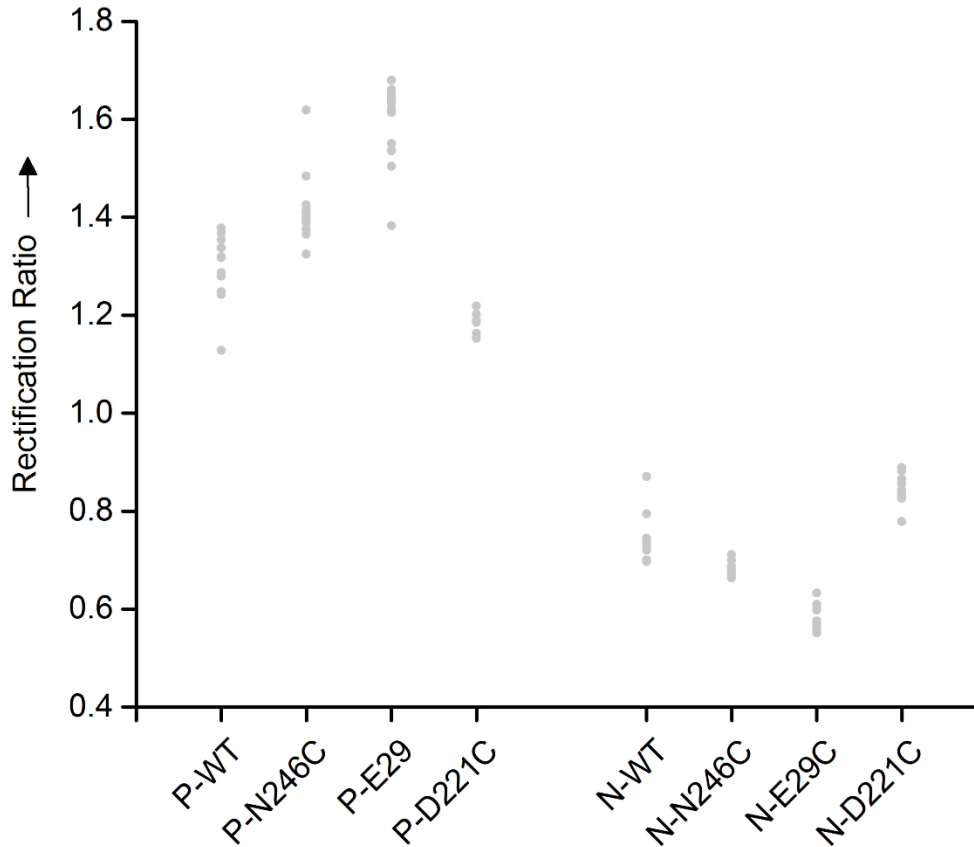


Figure S1. Unitary conductance versus applied potential for WT OmpF. OmpF trimers in 1% (w/v) β OG were reconstituted into planar DPhPC bilayers by addition to the *cis* compartment. Each point represents a mean unitary conductance value (\pm standard deviation) for OmpF in the P or N orientation (P-OmpF, $n = 12$; N-OmpF, $n = 12$) in 0.1 M KCl, 20 mM potassium phosphate buffer, pH 7.0.



	WT	N246C	E29C	D221C
P-OmpF	1.3 ± 0.1	1.4 ± 0.1	1.6 ± 0.1	1.2 ± 0.1
N-OmpF	0.75 ± 0.06	0.68 ± 0.04	0.57 ± 0.04	0.84 ± 0.03

Figure S2. Scatter plot of rectification ratios from individual WT and OmpF mutant channels. Each point represents the rectification ratio ($I_{+100\text{mV}}/I_{-100\text{mV}}$) of a single WT or mutant channel inserted into the bilayer in a P- or N-OmpF orientation. The average rectification ratios (\pm standard deviation) were as follows: 1.3 ± 0.1 (P-WT, $n = 12$), 1.4 ± 0.1 (P-N246C, $n = 15$), 1.6 ± 0.1 (P-E29C, $n = 16$), 1.2 ± 0.1 (P-D221C, $n = 5$) and 0.75 ± 0.06 (N-WT, $n = 12$), 0.68 ± 0.04 (N-N246C, $n = 14$), 0.57 ± 0.04 (N-E29C, $n = 18$), 0.84 ± 0.03 (N-D221C, $n = 15$).

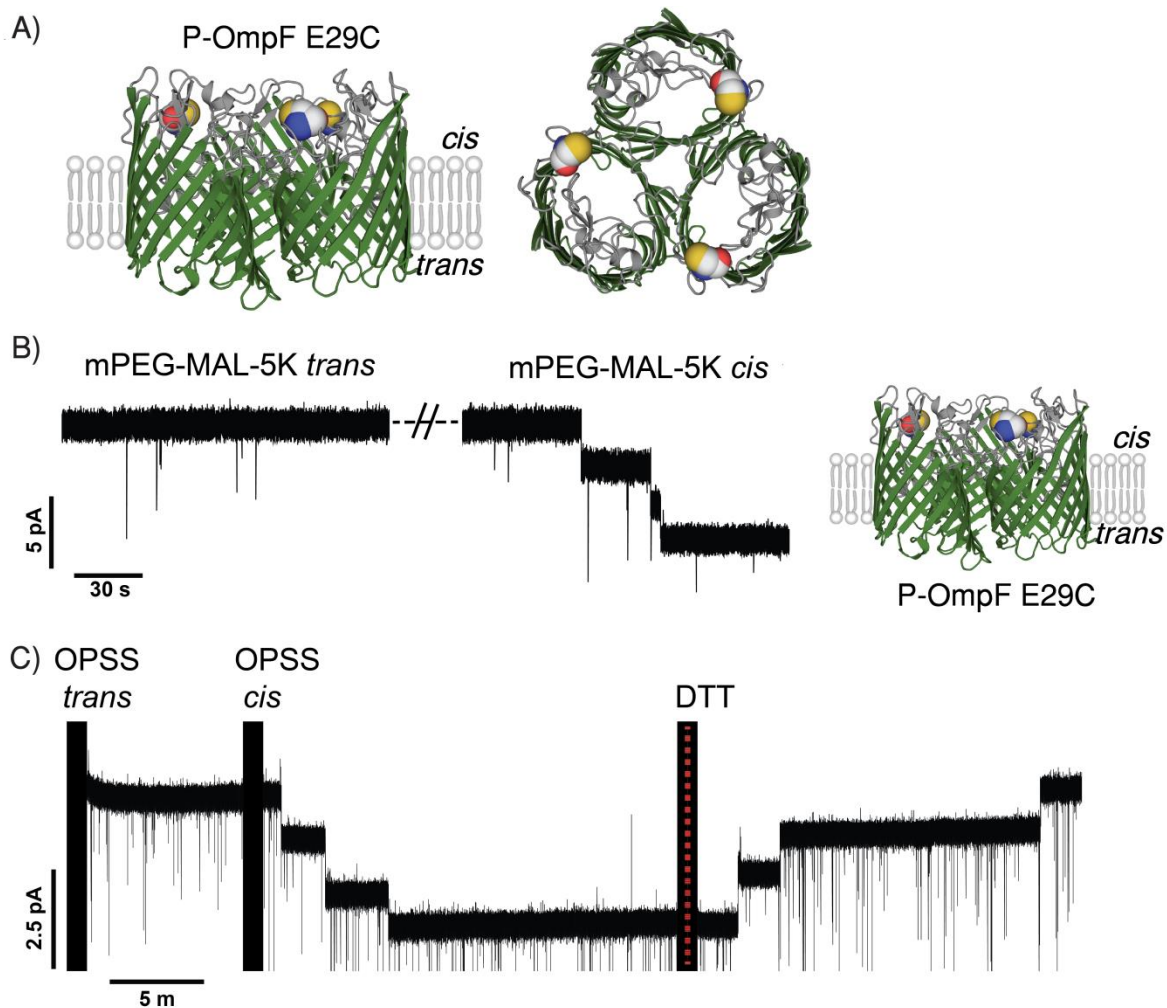


Figure S3. Extracellular mutant E29C. A) Structure of OmpF E29C generated in PyMOL from the wild-type crystal structure (PDB: 2OMF). The E29C mutation located on extracellular loop 1 of each subunit is highlighted as a sphere (left). Extracellular view (right). B) Sequential addition of mPEG-MAL-5K to the *trans* and then the *cis* side of the bilayer of a P-OmpF channel. Addition of mPEG-MAL-5K (1 mM) to the *trans* side of the bilayer did not produce a stable drop in current. A three-step drop in pore conductance was observed only when the reagent was introduced to the *cis* side of the bilayer. The orientation that follows from the sidedness of the reaction is shown on the right. C) Sequential addition of mPEG-OPSS-5K to the *trans* and then the *cis* side of a bilayer containing a single P-OmpF porin. A three-step drop in pore conductance was observed only when the mPEG-OPSS-5K (1 mM) was introduced to the *cis* side of the bilayer. The reaction was reversed in three steps by treatment with DTT (20 mM). The applied potential in the recordings was +70 mV.

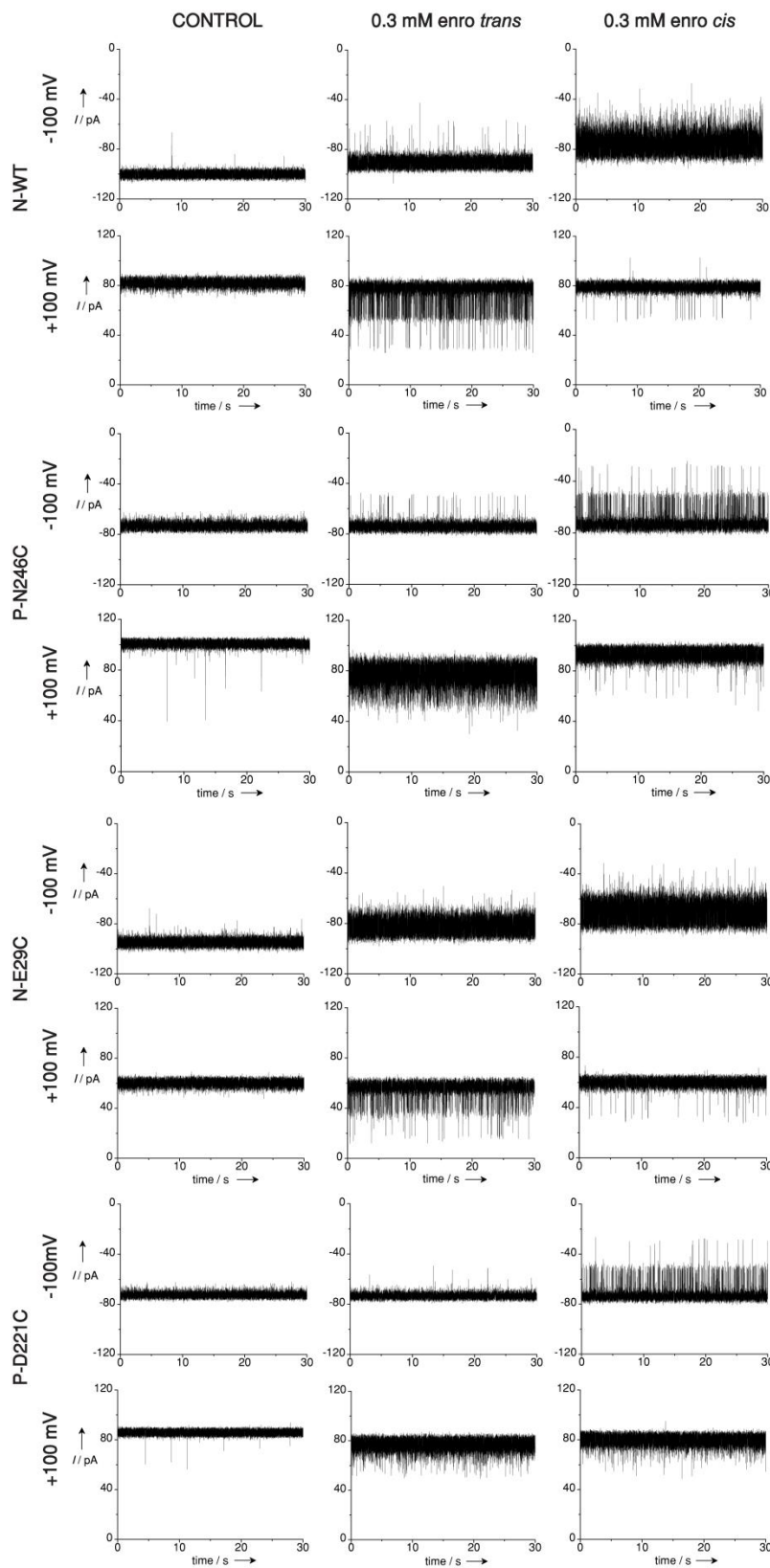


Figure S4. Representative segments of current traces from a single OmpF WT or mutant pore in the presence of enrofloxacin and Mg^{2+} . The buffer was 0.1 M KCl, 20 mM potassium phosphate, pH 7.0, 5 mM $MgCl_2$. Recordings were made at -100 mV and $+100$ mV without antibiotic (left column), with 0.3 mM enrofloxacin on the *trans* side (middle column), and with 0.3 mM enrofloxacin on the *cis* side (right column). Pores in the P-OmpF orientation showed an increase in fast flickering after the *trans*-side addition of enrofloxacin at $+100$ mV, compared to *cis*-side addition, and slow binding events after *cis*-side addition at -100 mV. Pores in the N-OmpF orientation showed increased flickering when enrofloxacin was introduced on the *cis* side of the bilayer at -100 mV and slow binding events upon *trans*-side addition at $+100$ mV. This inverted behavior enforces the hypothesis that the current-voltage asymmetries denoted as P- and N-OmpF represent pores in opposite orientations and shows that the cysteine mutants maintain the same directionality as the WT for both types of current-voltage asymmetry.

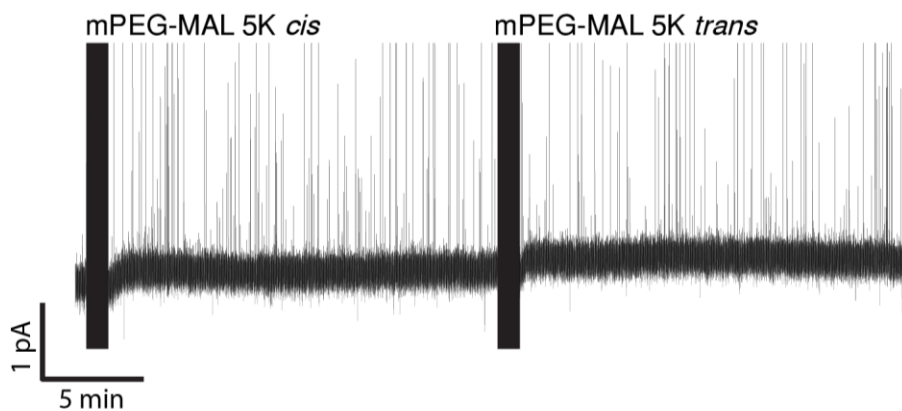


Figure S5. Asymmetric addition of mPEG-MAL-5K to WT OmpF. mPEG-MAL-5K (1 mM) was sequentially added to the *cis* and then to the *trans* side of a single WT channel in the P-OmpF orientation. The buffer was 0.1 M KCl, 20 mM potassium phosphate, pH 7.0. The reaction was allowed to proceed for 20 minutes after each addition. No current steps were observed, indicating that no reaction occurred from either side.

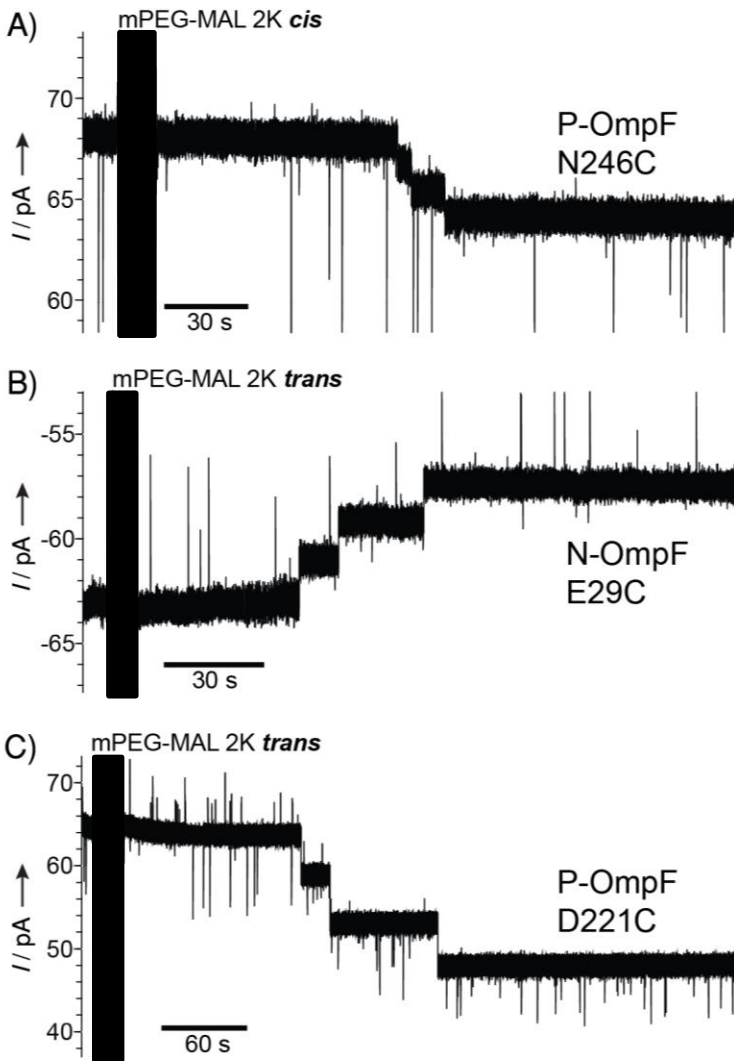


Figure S6. Asymmetric addition of mPEG-MAL-2K to OmpF cysteine mutants. Single-channel current traces from P-OmpF and N-OmpF pores after the addition of mPEG-MAL-2K (1 mM) to the recording chamber. A) An N246C pore in the P-OmpF orientation showed a three-step decrease in conductance only when mPEG-MAL-2K was introduced on the *cis* side of the bilayer. B) An E29C pore in the N-OmpF orientation reacted with mPEG-MAL-2K only when it was introduced on the *trans* side of the bilayer. C) A P-OmpF D221C pore reacted with mPEG-MAL-2K only when it was introduced on the *trans* side of the bilayer. Potentials of +70 mV (P-OmpF) and -70 mV (N-OmpF) were applied to keep the current flow in the same direction with respect to the pore.

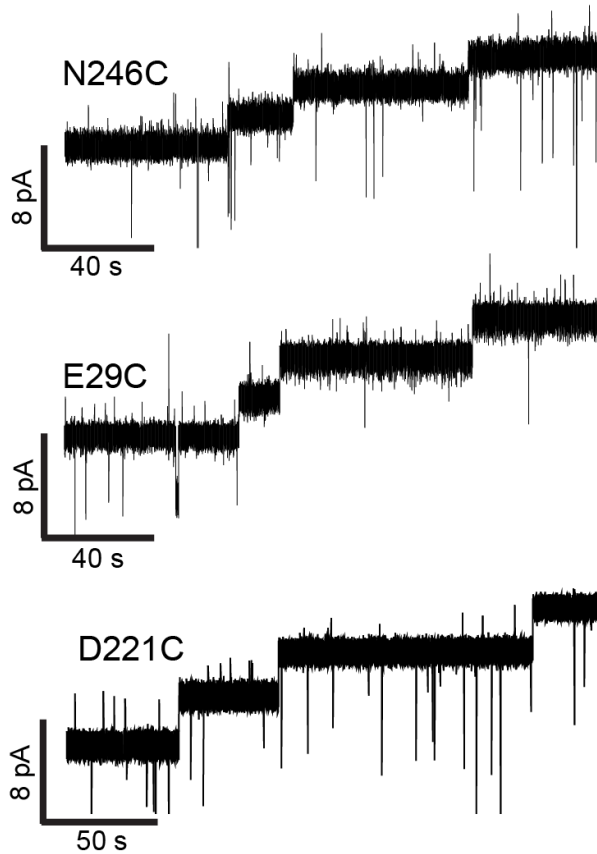


Figure S7. Asymmetric addition of 2-methylsulfonylsulfanyethanesulfonate (MTSES) to OmpF cysteine mutants. The buffer was 0.1 M KCl, 20 mM potassium phosphate, pH 7.0. Reaction of P-OmpF cysteine mutant channels with MTSES (1 mM) added to the *cis* or *trans* side of the bilayer caused conductance *increases*. The average conductance increase per step was 1.9 ± 0.8 pA ($n = 2$) for N246C, 1.1 ± 0.1 pA ($n = 4$) for E29C, and 3.2 ± 0.8 pA ($n = 2$) for D221C. All recordings were performed at +70 mV.

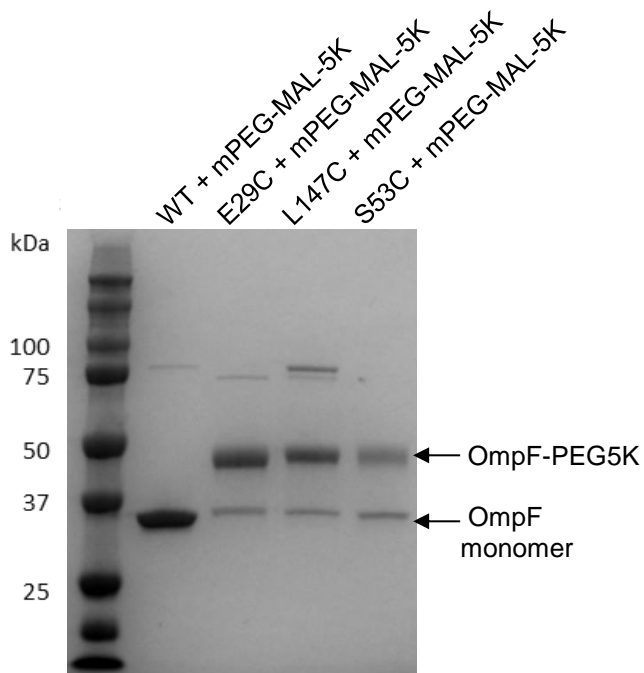


Figure S8. SDS-PAGE of OmpF E29C, L147C and S53C after reaction with with mPEG-MAL-5K. All lanes contain OmpF monomer (35 μ g) reacted with mPEG-MAL-5K (1 mM) dissolved in recording buffer before protein prior to denaturation. Monomer was obtained by heating the protein at 80°C for 10 min in 1% SDS prior to loading on the gel. The attachment of PEG-5K to an OmpF monomer produces a shift on the gel (band marked OmpF-PEG5K). Unreacted OmpF monomer appears as a single band, and a trimer band of lower mobility is also visible.

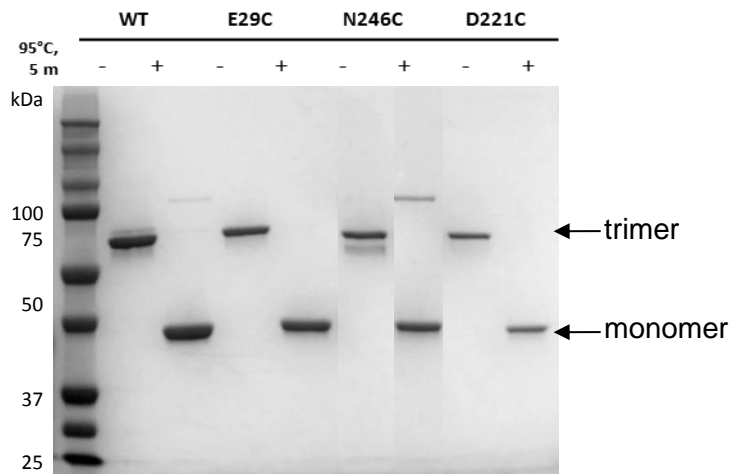


Figure S9. Heat stability of OmpF WT and cysteine mutants. The electrophoretic behavior of OmpF WT and mutants E29C, N246C, D221C was assessed by SDS-PAGE. Protein was either heated at 95°C for 5 minutes in the presence of β -mercaptoethanol or not heated, prior to loading on a 10% Mini-PROTEAN® gel (Bio-Rad) run at 200 V.